

Angular Dependence of the Spin Photocurrent in a Co-Fe-B/MgO/*n-i-p* GaAs Quantum-Well Structure

Laipan Zhu,^{1,5} Wei Huang,^{1,2} Pierre Renucci,⁴ Xavier Marie,⁴ Yu Liu,^{1,2} Yuan Li,^{1,2} Qing Wu,^{1,2} Yang Zhang,^{1,2} Bo Xu,^{1,2} Yuan Lu,^{3,†} and Yonghai Chen^{1,2,*}

¹Key Laboratory of Semiconductor Materials Science, Beijing Key Laboratory of Low Dimensional Semiconductor Materials and Devices, Institute of Semiconductors, Chinese Academy of Sciences, Beijing 100083, China

²College of Materials Science and Opto-Electronic Technology, University of Chinese Academy of Sciences, Beijing 100049, China

³Institut Jean Lamour, UMR 7198, CNRS-Université de Lorraine, BP 239, 54506 Vandœuvre, France

⁴Université de Toulouse, INSA-CNRS-UPS, LPCNO, 135 Avenue de Rangueil, F-31077 Toulouse, France

⁵Beijing Institute of Nanoenergy and Nanosystems, Chinese Academy of Sciences, Beijing 100083, China
(Received 20 July 2017; revised manuscript received 11 October 2017; published 20 December 2017)

We evidence at room temperature the detection of photogenerated spin currents by using a magnetic electrode without the need of an external magnetic field. The device is based on a semiconductor (Al, Ga)As/GaAs quantum well embedded in a *p-i-n* junction. The spin filtering is performed owing to a Co-Fe-B/MgO electrode with in-plane magnetization. We observe a helicity-dependent photocurrent when the device is excited under oblique incidence with circularly polarized light. The helicity-dependent photocurrent is explored as a function of the incident and azimuth angles of the incoming light wave vector with respect to the magnetization direction of the magnetic electrode. The results are interpreted as a consequence of the photogenerated average electron spin under oblique incidence in a quantum well governed by optical selection rules involving electron-heavy-hole and electron-light-hole transitions. A systematic study of the helicity asymmetry as a function of the photon energy and applied bias is performed. It demonstrates that this asymmetry is at its maximum close to the GaAs quantum well and (Al,Ga)As bulk optical transitions. The asymmetry can be controlled by an external bias on the structure. Finally, we show that this asymmetry decreases when the temperature increases.

DOI: 10.1103/PhysRevApplied.8.064022

I. INTRODUCTION

Spintronic devices based on spin-polarized electrons offer the promise of significant advances in device performance in terms of speed, size, and power consumption [1–3]. In a spin light-emitting diode (spin LED) [4–9], solid-state information stored within ferromagnetic materials can be transferred into circularly polarized photons emitted via carrier-photon angular momentum conversion. Several advanced semiconductor technologies have been proposed. Potential devices ranging from a memory element with optical readout and optical transport of spin information [10], advanced optical switches [11], circularly polarized single-photon emitters for quantum cryptography [12] to chiral analysis [13], and three-dimensional display screens [14] are anticipated. By reversing the operation condition of spin LED, one can also realize the spin photodiode function by illuminating the device with circularly polarized light and obtain the helicity asymmetry

(or conversion efficiency) of the photocurrent [15,16]. Several research groups have investigated the possibility of detecting a spin-polarized photocurrent generated under circularly polarized light using metal-oxide-semiconductor structures or spin LED structures [17–20]. As the photocurrent can be measured even at room temperature, it opens the way for promising applications in spin detectors of circularly polarized light [20] and spin filters [21–23]. When the spin-polarized photocurrents are detected under an external magnetic field [17–20], it is hard to distinguish the spin-related effect from the magnetic circular dichroism (MCD) of the magnetic layer as well from the artifact due to the Zeeman splitting in the semiconductor part [24]. Up to now, there were very few attempts to work at zero external magnetic field. The first one was based on the use of a thick perpendicular magnetic injector to get rid of this Zeeman-effect-based artifact [25]. Very recently, Roca *et al.* [15] proposed a helicity-dependent photocurrent under a given laser oblique incidence to work without an external magnetic field on a metal-oxide semiconductor based on Fe/Al₂O₃/p-doped GaAs with in-plane magnetization. Nevertheless, a systematic study of the influence of the incident and azimuth angles on the amplitude of the helicity asymmetry of the photocurrent is still missing. In addition,

*Corresponding author.
yhchen@semi.ac.cn

†Corresponding author.
yuan.lu@univ-lorraine.fr

most of the former studies of the role of the external bias on the amplitude of the helicity asymmetry were carried out at a fixed excitation wavelength [18–21], so it was not possible to distinguish between the exact influence of the bias on the helicity asymmetry and the influence of the Stark effect [26] on the energy levels in the semiconductor part.

In this paper, we use a spin-LED-like device to detect at room temperature photogenerated spin currents due to a magnetic electrode without the need of an external magnetic field by exciting the structure with a tilted incident angle. First, we investigate in a systematical way the influence of the incident and azimuth angles of the incoming light wave vector (with respect to the magnetization direction of the magnetic electrode) on the helicity asymmetry of the photocurrent. Second, this asymmetry is explored as a function of the wavelength of excitation. Our results are in good agreement with the theory that allows us to calculate the photogenerated average electron spin under oblique incidence in quantum wells predicted by optical selections rules. Finally, we also study the influence of the external bias and the temperature on the photocurrent asymmetry. We suggest a possible way to interpret these results based on the Dyakonov-Perel (DP) spin-relaxation mechanism [27] and on the requirement of the existence of a recombination channel for electron spins whose orientation is opposite the magnetization of the electrode.

II. SAMPLE PREPARATION AND CHARACTERIZATION

The sample structure is sketched in Fig. 1(a). It consists in a spin LED where a GaAs/(Al,Ga)As quantum well (QW) is embedded in the intrinsic region of the p - i - n junction surmounted by a Co-Fe-B/MgO electrode.

The quantum-well p - i - n structure and the tunnel barrier are grown by molecular beam epitaxy (MBE), while the ferromagnet contact is deposited by sputtering. The p - i - n structure has the following layers: A 300-nm p -GaAs:Be ($p = 2.17 \times 10^{19} \text{ cm}^{-3}$) buffer layer is initially deposited on (001) p -GaAs:Zn ($p = 2 \times 10^{19} \text{ cm}^{-3}$) substrate, followed by a 500-nm p -Al_{0.08}Ga_{0.92}As ($p = 2 \times 10^{19} \text{ cm}^{-3}$) layer. Then, a single quantum well of 50-nm undoped Al_{0.08}Ga_{0.92}As/10-nm undoped GaAs QW/50-nm undoped Al_{0.08}Ga_{0.92}As and a 50-nm n -(Al,Ga)As:Si ($n = 1 \times 10^{16} \text{ cm}^{-3}$) cap layer are deposited in turn. The surface of the p - i - n structure is passivated with arsenic in the III-V MBE chamber and then transferred through the air into another MBE-sputtering interconnected system. The arsenic capping layer is first desorbed at 300 °C by monitoring *in situ* reflection high-energy electron-diffraction patterns in the MBE chamber, and after that, a 2.5-nm MgO tunneling barrier layer is grown at 250 °C. The sample is then transferred to the sputtering chamber to grow a 3-nm Co₄₀Fe₄₀B₂₀ ferromagnetic layer. Finally, 5-nm Ta is deposited to prevent oxidation. The 300- μm -diameter circular mesas are then processed using standard UV photolithography and etching techniques.

The optical microscopy images, I - V characteristics, and circularly polarized electroluminescence of the measured device are shown in Fig. S1 in the Supplemental Material [28]. A high-resolution transmission-electron-microscopy image (HRTEM) shown in Fig. 1(b) reveals a smooth and sharp MgO/(Al,Ga)As interface. Moreover, the continuity of the 3-nm Co-Fe-B layer can also be validated in the HRTEM image performed by using a JEOL ARM200 cold field-emission gun working at 200 kV. A mode-locked Ti:sapphire laser with a repetition rate of 80 MHz and a pulse width of 140 fs serves as the excitation source.

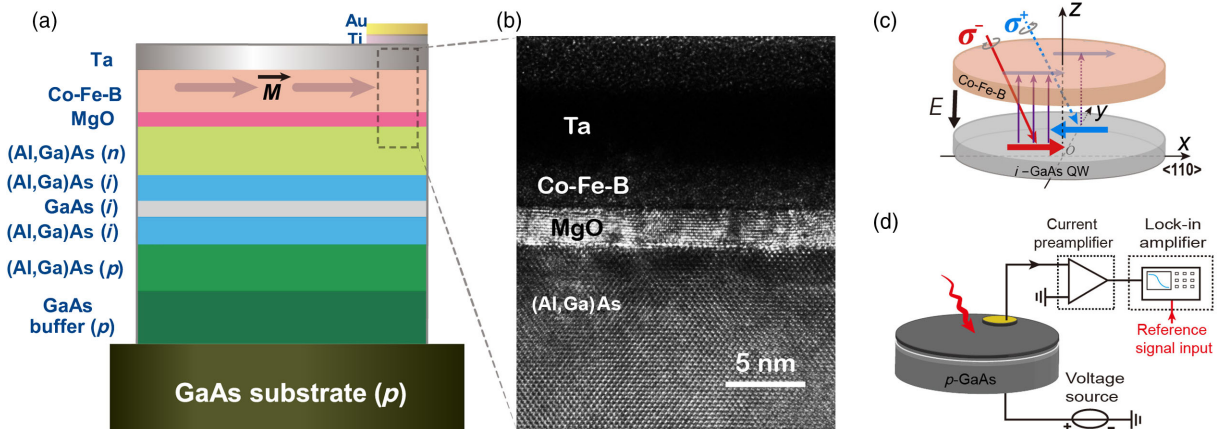


FIG. 1. Sample structure and photocurrent measurement. (a) The schematic diagram of the cross section of the device. The black bold arrows in Co-Fe-B denote the orientation of the remanent magnetic moment. (b) HRTEM image of the MgO/Co-Fe-B/Ta spin detector on (Al,Ga)As-based LED structure. (c) Schematic of the difference of photocurrent between right and left circularly polarized light with oblique incidence thanks to a selective spin filtering by the Co-Fe-B/MgO layer. The red and blue horizontal arrows correspond to S_x , the projection along x of the photogenerated average spin S for σ^- and σ^+ , respectively. (d) Schematic diagram of the electrical measurement under bias.

The excitation wavelength is tuned from 700 to 870 nm, which covers the excitation energy of the first valence subband of heavy holes to the first conduction subband and the first valence subband of light holes to the first conduction subband (LH1- ϵ 1) transitions in the GaAs QW. The spot diameter and average power of the laser are 2 mm and 0.2 mW, respectively. The incident light goes through a polarizer and a photoelastic modulator (PEM) whose retardation is set to be 0.25λ to yield a modulated circularly polarized light with a fixed modulating frequency at 50 KHz. We measure the helicity-dependent photocurrent ΔI that is related to the difference of the photocurrent between the right and left circularly polarized light ($\Delta I \propto I^{\sigma^+} - I^{\sigma^-}$) due to a selective spin filtering of the Co-Fe-B/MgO [see Fig. 1(c)]. A low-noise-current preamplifier and a lock-in amplifier synchronized with the 50-KHz signal of the PEM are used. We also measure $I_{ph}[\propto (I^{\sigma^+} + I^{\sigma^-})/2]$ that is the total photoinduced current. This total current is accurately measured by the low-noise-current preamplifier and a lock-in amplifier synchronized with the 220-Hz signal of an optical chopper. In this work, we study the azimuth angle, the incident angle, the temperature, and the external bias dependence of the amplitude of the helicity asymmetry of the photocurrent. In the measurements, positive bias corresponds to the cathode (+) of the voltage source connected with the bottom electrode, whereas for negative bias, the cathode of the voltage source is connected with the top electrode, as schematically shown in Fig. 1(d). We define the photocurrent helicity asymmetry F (figure of merit) as $F = (\Delta I/I_{ph})$. We mainly discuss I_{ph} and F in the following, and the measured ΔI are presented in Figs. S2, S4, and S5 in the Supplemental Material [28].

III. RESULTS AND DISCUSSION

A. Influence of the azimuth and incidence angles on the photocurrent helicity asymmetry

First, the excitation wavelength is fixed at 825 nm close to the energy of the LH1 - ϵ 1 transition in the GaAs QW at

300 K. In the inset of Figs. 2(a) and 2(c), we show the schematic diagram of the illumination configurations. Here, we define θ as the angle between the incident light and the out-of-plane direction of the sample. We define α as the angle between the projection direction of the incident light and the direction of the remanent magnetic moment of Co-Fe-B; the preferred magnetic orientation is along the $\langle 110 \rangle$ direction of the GaAs substrate. First, we study the azimuth angle (α) dependence of the helicity asymmetry of the photocurrent with incident angle $\theta = 30^\circ$ at 300 K, as shown in Figs. 2(b) and 2(b). Remarkably, the azimuth angle α dependence of F shows a cosinelike behavior at three different bias voltages. From Fig. 2(b), we can see that F exhibits maximal values when $\alpha = 0^\circ$, while F reverses its sign when $\alpha = 180^\circ$. As expected, F almost vanishes when $\alpha = 90^\circ$.

Second, we study the photocurrent as a function of the incident angle θ for $\alpha = 0^\circ$ at 300 K, as shown in Figs. 2(c) and 2(d), and Fig. S2 (Supplemental Material [28]). From Fig. 2(d), we can see that the calculated helicity asymmetry F changes quasilinearly with the incident angle at three different bias voltages. Other incident angles' ($\theta = 0^\circ, -30^\circ$) and azimuth angles' ($\alpha = 90^\circ, 180^\circ$) dependence of F at 300 K are shown in Fig. S3 in the Supplemental Material [28]. We can see a clearly vanished F when $\theta = 0^\circ$ [see Fig. S3(a) in the Supplemental Material [28]] or $\alpha = 90^\circ$ [see Fig. S3(c) in the Supplemental Material [28]]. The azimuth angle α dependence of F with incident angle $\theta = -30^\circ$ shows, however, a negative cosinelike behavior at three different bias voltages [see Fig. S3(b) in the Supplemental Material [28]]. From Fig. S3(d) in the Supplemental Material [28], with azimuth angle $\alpha = 180^\circ$, we can see that the calculated helicity asymmetry F also changes quasilinearly with the incident angle at three different bias voltages, while the sign of the slope of the fitting line is opposite compared to the case of azimuth angle $\alpha = 0^\circ$ shown in Fig. 2(d).

These results can be well understood if we consider the simple phenomenological model described in the following.

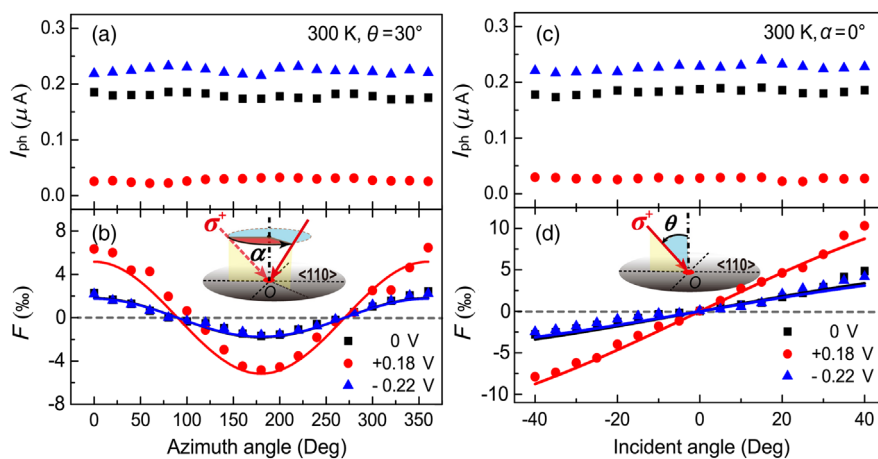


FIG. 2. Total photocurrents and helicity asymmetry as a function of the azimuth and incidence angle. (a) The total photo-induced direct currents and (b) the helicity asymmetry of the photocurrents changing with the azimuth angle for the incident angle $\theta = 30^\circ$ under three different bias voltages at 300 K. The solid lines correspond to cosine fitting. (c) The total photo-induced currents and (d) the helicity asymmetry changing with incidence angle with the azimuth angle $\alpha = 0^\circ$ under three different bias voltages at 300 K. The solid lines correspond to the sine fitting. The insets in (b) and (d) illustrate the definition of the azimuth angle and the incident angle, respectively.

The helicity asymmetry can be written as $F = CP_{\text{FM}}S_x$, where P_{FM} is the spin polarization of the ferromagnetic layer at the Fermi level, S_x is the projection on the magnetization direction $\langle 110 \rangle$ (that we call the x direction for the sake of simplicity) of the electron spin S photogenerated by the laser [see Fig. 1(c)]. C is a nontrivial function depending on many parameters: $\tau_{s,\text{QW}}$ the electron spin-relaxation time in the GaAs quantum well, τ_{esc} the escape time from the well, τ the electron radiative recombination time in the QW, τ_s the spin relaxation time in the (Al,Ga)As bulk during the drift-diffusion process, τ_{bulk} the electron radiative recombination time in the bulk, t the tunneling time through MgO, and l the distance between the QW and the electrode. Note that the spin-relaxation time $\tau_{s,\text{QW}}$ in this type of [001] GaAs/(Al, Ga)As quantum well embedded in the p - i - n junction may depend on the applied bias. When no bias voltage is applied to the structure, and for a 10-nm QW with 8% of aluminum, this spin-relaxation time is about 525 ps at 80 K [29] and can be estimated from Ref. [30] around 70 ps at 300 K for a bare quantum well. The tunneling time out of the well depends mainly on the applied bias, on the confinement energy in the quantum well, and on the temperature. It can range from a few hundred picoseconds to a few picoseconds [31,32]. As calculated in Ref. [33] the electron spin S photogenerated in a quantum well by the laser under oblique incidence has a direction which depends on the heavy-hole–light-hole mixing in the valence band. S is in the incident plane defined by the normal to the quantum-well plane (z axis) and the incident light wave vector. As this incident plane is tilted by the angle α from the magnetization direction $\langle 110 \rangle$ (x axis), it is, thus, clear that S_x can be written as $S_x = \cos(\alpha)S_\alpha$, where S_α is the projection of S along the direction e_α defined by the intersection of the incident plane and the quantum-well plane. The second important point from Ref. [33] is that $S_\alpha = f(E_{\text{photon}}) \sin(\theta)$ where $f(E_{\text{photon}})$ is a function that contains optical selection rules for electron-heavy-hole and electron-light-hole transitions in a QW. So, F can be finally written as

$$F = CP_{\text{FM}} \cos(\alpha) f(E_{\text{photon}}) \sin(\theta). \quad (1)$$

The experimental dependence of F as a function of α is in very good agreement with this model, as shown in Fig. 2(b). The experimental dependence of F as a function of the incident angle θ is also very well reproduced. For θ varying from -40° to 40° , $\sin(\theta) \sim \theta$. The expected linear increase of F as a function of θ is indeed experimentally observed in Fig. 2(d), and Fig. S3(d) in the Supplemental Material [28].

Let us come back to the physical origin of the photo-generated in-plane spin component S_α . We consider a pure circular polarization with a wave vector tilted from the normal of the sample surface by the angle of incidence α . The corresponding mode can be decomposed in a combination of two modes, one propagating along the growth

axis of the structure and one propagating in plane. It is well known that the in-plane mode cannot photogenerate any spin if the only excited transition is the heavy-hole- $e1$ transition [34]. However, for laser energy above the QW absorption edge, the valence-band states are linear combinations involving both heavy-hole and light-hole states [35]. The weight of the light hole can be significant, particularly when the laser energy exceeds the energy of the light-hole- $e1$ transition in the center of the Brillouin zone. It is then possible to photogenerate spin with an in-plane mode thanks to this transition. Finally, taking into account the two modes, it is shown in Ref. [33] that it is possible to create an in-plane average spin component S_α in a direction that corresponds to the projection of the light wave vector on the plane of the quantum well.

B. Influence of the excitation wavelength and the bias voltage

We perform a systematic study of the spectra of ΔI and I_{ph} as a function of bias voltage at 80 K [see Fig. S4 in Supplemental Material [28] and Fig. 3(a)], where $\theta = 0^\circ$ and $\alpha = 15^\circ$. We then deduce the spectra of helicity asymmetry at 80 K [see Fig. 3(b)]. In Figs. 3(b) and 3(b), we identify clearly the energy positions corresponding to the optical transitions in the i -GaAs QW at approximately 820 nm and the (Al,Ga)As barrier at approximately 775 nm. It corresponds pretty well to the calculated transitions based on a six-band $k \cdot p$ model that gives heavy-hole-electron and light-hole-electron transition wavelengths, respectively [33,36]. It also demonstrates that this asymmetry is at its maximum close to the GaAs quantum well and (Al,Ga)As bulk optical transitions. With the voltage varying from +0.25 to -0.216 V, the peak positions corresponding to the transition of i -GaAs QW for I_{ph} reveal an obvious quantum red Stark shift [see Fig. 3(a)], which is a normal rule for the total photocurrent under bias [26]. Interestingly, between the i -GaAs QW and (Al,Ga)As barrier, there are still small peaks between the energy positions of the (Al,Ga)As and i -GaAs QW, which is probably derived from the interface states [37,38] between Co-Fe-B and MgO or due to a possible Franz-Keldysh effect [39]; further works should be done in the future to confirm these hypotheses. The influence of the bias on the helicity asymmetry F related to the i -GaAs QW is shown in Fig. 3(c). The helicity asymmetry is measured at the wavelength corresponding to the quantum-well absorption maximum for a given bias. We measure an increase of the helicity asymmetry with positive biases, while a decreased amplitude of the helicity asymmetry is observed with negative biases. Two mechanisms can explain this behavior.

1. Bias dependence of the electron spin-relaxation time

A dependence of the electron spin-relaxation time with the applied bias can be considered. It could be linked to the

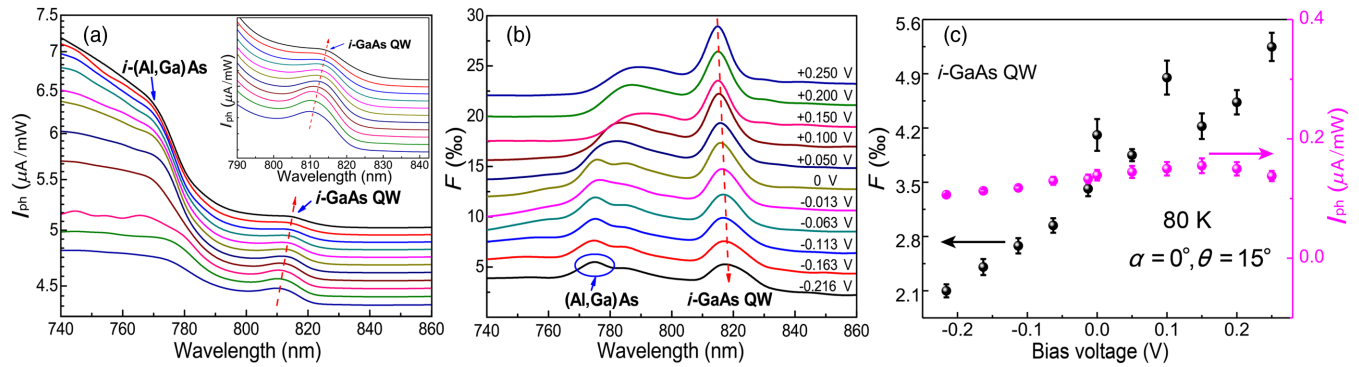


FIG. 3. Bias voltage dependence of the spectra of total photocurrents and helicity asymmetry at 80 K. (a) Spectra of the total photoinduced direct currents. Inset: Enlargement of the quantum-well transition. (b) Spectra of the helicity asymmetry at different bias voltages at 80 K. Note that the spectra in (a) and (b) are intentionally shifted for clarity, and the color coding is the same for (a) and (b). (c) The helicity asymmetry of the photocurrent and the total photoinduced direct current as a function of bias voltage corresponding to the transition of the *i*-GaAs QW, respectively. The azimuth and incident angles in these experiments are fixed to be 0° and 15° , respectively.

Rashba effect on the Dyakonov-Perel electron spin-relaxation time in the quantum well [40]. The electron spin-relaxation time varies if the amplitude of the electric field increases as observed in the (001) and (111) GaAs quantum wells [41,42]. For the (001) QW investigated in this paper, we can expect that the flatter the bands are for the quantum well, the longer the electron spin-relaxation time is. In our device, we can estimate a built-in electric field of 120 kV/cm. For such a large electric field, the electron spin-relaxation time decreases when the electric field increases (in absolute value) [43]. This can explain the measured helicity asymmetry increase with positive biases and its decreasing amplitude for negative biases.

2. Recombination channel for the electron spin orientation opposite the magnetization

Another mechanism can explain the measured bias dependence. In order to get a difference between the two photocurrents under right and left circularly polarized light, a recombination channel to “kill” electrons with a spin opposite the magnetization is needed [17]. Note that obtaining a spin-dependent photocurrent relies on both a spin-dependent transmission coefficient at the ferromagnet-semiconductor interface and an efficient recombination of the reflected minority-spin carriers in the semiconductor

[16,17,44]. In one case for the $V < 0$ bias [see Fig. 4(a)], the bands will be heavily tilted, so the electron’s “killing” channel (radiative recombination) is almost closed. In contrast, a reversal of the bias leading to almost flat band conditions will open the electron’s killing channel (radiative recombination), as shown in Fig. 4(b). This physical model can explain why we have to work with $V > 0$ to evidence significant helicity asymmetry for the photocurrent [see Fig. 3(c)]. Note that there are two advantages of using a quantum well as an optical absorber in the device. First, it opens the way in the future for an optimization of the electron spin-relaxation time in the active region. The latter electron spin-relaxation time can be controlled by engineering the QW. One can imagine, for example, to benefit from the internally built electric field produced by the piezoelectric effect as it is shown in strained (In, Ga)As/GaAs quantum wells grown along the [111] direction [45] in order to compensate for the Dresselhaus term by the Rashba one and, thus, strongly damp the corresponding spin-relaxation mechanism [42]. The second advantage of using a quantum well is to offer an efficient recombination channel for electron spins whose orientation is opposite the magnetization of the electrode. The efficiency of this recombination channel can be tuned by the applied bias.

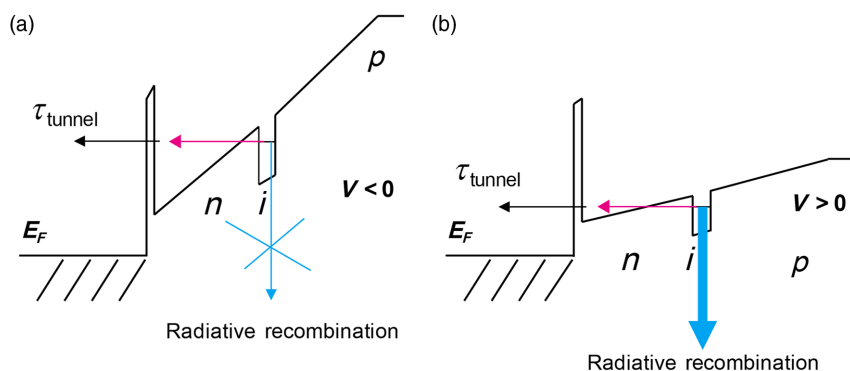


FIG. 4. Schematic diagrams of the energy band under bias. (a) Tilted bands under a negative-bias voltage with electron’s killing channel (radiative recombination) almost closed. (b) Almost flat band conditions under a positive-bias voltage with the electron’s killing channel (radiative recombination) open.

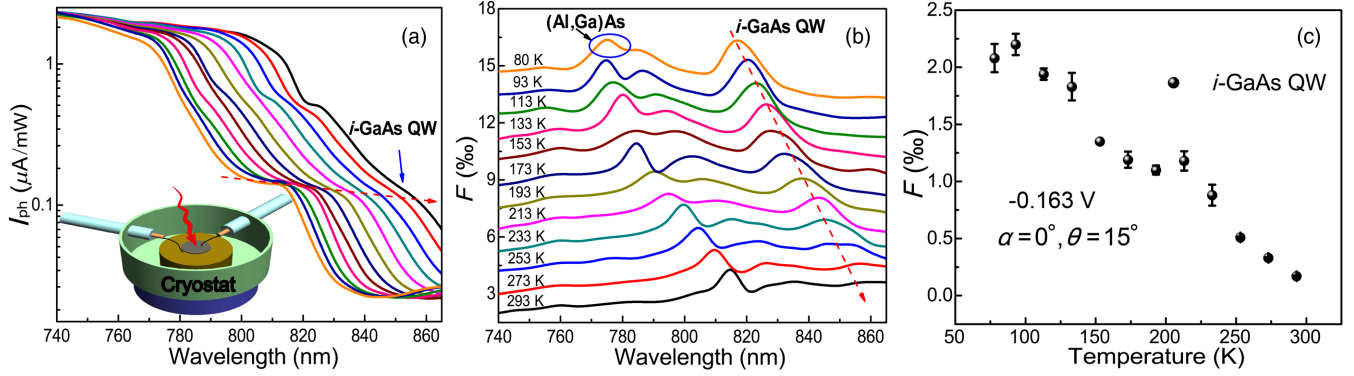


FIG. 5. Temperature dependence of the spectra of total photocurrents and helicity asymmetry under -0.163 -V bias. (a) Spectra of the common photoinduced direct currents, whose color coding is the same as Fig. 5(b). The inset is a schematic diagram of the cryostat for temperature control. (b) Spectra of the helicity asymmetry at different temperatures. Please note that the spectra are intentionally shifted for clarity. (c) The amplitude of helicity asymmetry as a function of the temperature corresponding to the transition of the i -GaAs QW. The bias voltage and the azimuth and incident angles in these experiments are fixed to be -0.163 V, 0° , and 15° , respectively.

C. Influence of the temperature

The temperature dependence of the spectra of ΔI , I_{ph} , and the deduced helicity asymmetry F with a fixed bias of -0.163 V are shown in Figs. 5(a) and 5(b), where $\theta = 0^\circ$ and $\alpha = 15^\circ$ (see, also, Fig. S5 in the Supplemental Material [28]). The energy corresponding to the i -GaAs QW shows a redshift with the increase of the temperature [Fig. 5(a)], which is simply due to the temperature dependence of the band gap. The temperature dependence of the helicity asymmetry of the photocurrent for i -GaAs QW can then be extracted [Fig. 5(c)]. We clearly observe a reduction of the helicity asymmetry with the increase of the temperature. This effect can be well explained by the reduction of the quantum-well DP electron spin-relaxation time when the lattice temperature increases, as it is clearly evidenced in Ref. [30]. We extract the temperature dependence of the peak position of the helicity asymmetry corresponding to the optical transition of i -GaAs QW (see Fig. S6 in the Supplemental Material [28]), which shows an almost linear increase of F with the decrease of the temperature by following the Varshni law.

D. Possible influence of magnetic circular dichroism

Finally, we discuss the possible artifacts in the measurements. First, when a magnetic field is applied, the absorption spectra for σ^+ and σ^- light are shifted due to the Zeeman effect in the quantum well [17]. So, for a given excitation wavelength, these two absorptions can be different, yielding a helicity-dependent current not related to the filtering of electron spins by the FM layer. This effect can be neglected in our experiments since (i) no external magnetic field is applied, and (ii) the stray field induced by the FM layer can be estimated to be less than 1 mT in the quantum-well plane [46,47]. The second type of possible artifact is the MCD due to the magnetic layer. Though a small MCD effect was reported for tilted excitation and

in-plane magnetization [15], it should not be sensitive to the bias voltage, and it should not exhibit a resonance with the quantum-well level and the (Al,Ga)As barrier gap, as we clearly observe. We conclude that MCD effects are also negligible in our measurements.

IV. CONCLUSIONS

We detect at room temperature photogenerated spin currents by using a magnetic electrode without the need of an external magnetic field. A clear helicity asymmetry is evidenced. The dependence of this asymmetry on the incident and azimuth angles of the incoming light wave vector in i -GaAs quantum well is interpreted as a consequence of the photogenerated average electron spin under oblique incidence in the quantum well governed by the optical selection rules. We also show that the asymmetry can be controlled by an applied bias. The temperature dependence is measured and interpreted on the basis of the Dyakonov-Perel spin-relaxation time in the quantum well. As the measured amplitude of the photocurrent asymmetry is weak, improvements are clearly required [particular attention can be paid to optimizing (i) the electron spin-relaxation time in the semiconductor part and (ii) tuning the efficiency of the recombination channel for carriers with spin opposite the magnetization direction of the electrode] in order to use such systems as efficient spin filters or polarization detectors in future spin-optronic applications.

ACKNOWLEDGMENTS

We thank Xavier Devaux for TEM characterization. The work is supported by the National Natural Science Foundation of China (Grants No. 61474114, No. 11574302, No. 11704032, and No. 61334006), the National Basic Research Program of China (Grants No. 2015CB921503 and No. 2013CB632805), National Key Research and Development Program (Grants

No. 2016YFB0402303 and No. 2016YFB0400101), and the China Postdoctoral Science Foundation (Grant No. 2016M600067). X.M. acknowledges Institut Universitaire de France. P.R. acknowledges the NEXT Grant No. ANR-10-LABX-0037 in the framework of the Programme des Investissements d'Avenir. Y.L. acknowledges the joint French National Research Agency-National Natural Science Foundation of China SISTER project (Grants No. ANR-11-IS10-0001 and No. NNSFC 61161130527) and the ENSEMBLE project (Grants No. ANR-14-0028-01 and No. NNSFC 61411136001).

L. Z. and W. H. contributed equally to this work.

-
- [1] G. A. Prinz, Magnetoelectronics, *Science* **282**, 1660 (1998).
- [2] S. Wolf, D. Awschalom, R. Buhrman, J. Daughton, S. Von Molnar, M. Roukes, A. Y. Chtchelkanova, and D. Treger, Spintronics: A spin-based electronics vision for the future, *Science* **294**, 1488 (2001).
- [3] I. Žutić, J. Fabian, and S. Das Sarma, Spintronics: Fundamentals and applications, *Rev. Mod. Phys.* **76**, 323 (2004).
- [4] R. Fiederling, M. Keim, G. Reuscher, W. Ossau, G. Schmidt, A. Waag, and L. Molenkamp, Injection and detection of a spin-polarized current in a light-emitting diode, *Nature (London)* **402**, 787 (1999).
- [5] Y. Ohno, D. Young, B. Beschoten, F. Matsukura, H. Ohno, and D. Awschalom, Electrical spin injection in a ferromagnetic semiconductor heterostructure, *Nature (London)* **402**, 790 (1999).
- [6] T. D. Nguyen, E. Ehrenfreund, and Z. V. Vardeny, Spin-polarized light-emitting diode based on an organic bipolar spin valve, *Science* **337**, 204 (2012).
- [7] P. Barate, S. Liang, T. T. Zhang, J. Frougier, M. Vidal, P. Renucci, X. Devaux, B. Xu, H. Jaffrès, J. M. George, X. Marie, M. Hehn, S. Mangin, Y. Zheng, T. Amand, B. Tao, X. F. Han, Z. Wang, and Y. Lu, Electrical spin injection into InGaAs/GaAs quantum wells: A comparison between MgO tunnel barriers grown by sputtering and molecular beam epitaxy methods, *Appl. Phys. Lett.* **105**, 012404 (2014).
- [8] B. S. Tao, P. Barate, J. Frougier, P. Renucci, B. Xu, A. Djéffal, H. Jaffrès, J. M. George, X. Marie, S. Petit-Watelot, S. Mangin, X. F. Han, Z. G. Wang, and Y. Lu, Electrical spin injection into GaAs based light emitting diodes using perpendicular magnetic tunnel junction-type spin injector, *Appl. Phys. Lett.* **108**, 152404 (2016).
- [9] V. G. Truong, P. H. Binh, P. Renucci, M. Tran, Y. Lu, H. Jaffrès, J. M. George, C. Deranlot, A. Lemaître, T. Amand, and X. Marie, High speed pulsed electrical spin injection in spin-light emitting diode, *Appl. Phys. Lett.* **94**, 141109 (2009).
- [10] R. Farshchi, M. Ramsteiner, J. Herfort, A. Tahraoui, and H. T. Grahn, Optical communication of spin information between light emitting diodes, *Appl. Phys. Lett.* **98**, 162508 (2011).
- [11] M. Holub and P. Bhattacharya, Spin-polarized light-emitting diodes and lasers, *J. Phys. D* **40**, R179 (2007).
- [12] P. Asshoff, A. Merz, H. Kalt, and M. Hetterich, A spintronic source of circularly polarized single photons, *Appl. Phys. Lett.* **98**, 112106 (2011).
- [13] J. Xu, A. Lakhtakia, J. Liou, A. Chen, and I. J. Hodgkinson, Circularly polarized fluorescence from light-emitting microcavities with sculptured-thin-film chiral reflectors, *Opt. Commun.* **264**, 235 (2006).
- [14] D.-Y. Kim, Potential application of spintronic light-emitting diode to binocular vision for three-dimensional display technology, *J. Korean Phys. Soc.* **49**, S505 (2006).
- [15] R. C. Roca, N. Nishizawa, K. Nishibayashi, and H. Munekata, Investigation of helicity-dependent photocurrent at room temperature from a Fe/ x -AlO $_x$ / p -GaAs Schottky junction with oblique surface illumination, *Jpn. J. Appl. Phys.* **56**, 04CN05 (2017).
- [16] M. Cantoni and C. Rinaldi, Light helicity detection in MOS-based spin-photodiodes: An analytical model, *J. Appl. Phys.* **120**, 104505 (2016).
- [17] P. Renucci, V. G. Truong, H. Jaffrès, L. Lombez, P. H. Binh, T. Amand, J. M. George, and X. Marie, Spin-polarized electroluminescence and spin-dependent photocurrent in hybrid semiconductor/ferromagnetic heterostructures: An asymmetric problem, *Phys. Rev. B* **82**, 195317 (2010).
- [18] A. F. Isakovic, D. M. Carr, J. Strand, B. D. Schultz, C. J. Palmstrøm, and P. A. Crowell, Optical pumping in ferromagnet-semiconductor heterostructures: Magneto-optics and spin transport, *Phys. Rev. B* **64**, 161304 (2001).
- [19] T. Taniyama, G. Wastlbauer, A. Ionescu, M. Tselepi, and J. A. C. Bland, Spin-selective transport through Fe/AlO $_x$ /GaAs(100) interfaces under optical spin orientation, *Phys. Rev. B* **68**, 134430 (2003).
- [20] S. Hovel, N. C. Gerhardt, M. R. Hofmann, F. Y. Lo, D. Reuter, A. D. Wieck, E. Schuster, W. Keune, H. Wende, O. Petravic, and K. Westerholt, Electrical detection of photo-induced spins both at room temperature and in remanence, *Appl. Phys. Lett.* **92**, 242102 (2008).
- [21] S. J. Steinmuller, C. M. Gürtler, G. Wastlbauer, and J. A. C. Bland, Separation of electron spin filtering and magnetic circular dichroism effects in photoexcitation studies of hybrid ferromagnet/GaAs Schottky barrier structures, *Phys. Rev. B* **72**, 045301 (2005).
- [22] G. Kirczenow, Ideal spin filters: A theoretical study of electron transmission through ordered and disordered interfaces between ferromagnetic metals and semiconductors, *Phys. Rev. B* **63**, 054422 (2001).
- [23] K. M. Alam and S. Pramanik, Spin filtering through single-wall carbon nanotubes functionalized with single-stranded DNA, *Adv. Funct. Mater.* **25**, 3210 (2015).
- [24] M. Oestreich and W. W. Rühle, Temperature Dependence of the Electron Landé g Factor in GaAs, *Phys. Rev. Lett.* **74**, 2315 (1995).
- [25] S. Hövel, N. C. Gerhardt, M. R. Hofmann, F.-Y. Lo, A. Ludwig, D. Reuter, A. D. Wieck, E. Schuster, H. Wende, W. Keune, O. Petravic, and K. Westerholt, Room temperature electrical spin injection in remanence, *Appl. Phys. Lett.* **93**, 021117 (2008).
- [26] H. Q. Le, J. J. Zayhowski, and W. D. Goodhue, Stark effect in Al $_x$ Ga $_{1-x}$ As/GaAs coupled quantum wells, *Appl. Phys. Lett.* **50**, 1518 (1987).

- [27] M. D'yakonov and V. Perel, Spin orientation of electrons associated with the interband absorption of light in semiconductors, *J. Exp. Theor. Phys.* **33**, 1053 (1971).
- [28] See Supplemental Material at <http://link.aps.org/supplemental/10.1103/PhysRevApplied.8.064022> for the optical-electrical properties of the device and the spectra and other angle dependence of the helicity-dependent photocurrent.
- [29] Y. Lu, V. G. Truong, P. Renucci, M. Tran, H. Jaffrès, C. Deranlot, J. M. George, A. Lemaître, Y. Zheng, D. Demaille, P. H. Binh, T. Amand, and X. Marie, MgO thickness dependence of spin injection efficiency in spin-light emitting diodes, *Appl. Phys. Lett.* **93**, 152102 (2008).
- [30] A. Malinowski, R. Britton, T. Grevatt, R. Harley, D. Ritchie, and M. Simmons, Spin relaxation in GaAs/Al_xGa_{1-x}As quantum wells, *Phys. Rev. B* **62**, 13034 (2000).
- [31] T. B. Norris, X. J. Song, W. J. Schaff, L. F. Eastman, G. Wicks, and G. A. Mourou, Tunneling escape time of electrons from a quantum well under the influence of an electric field, *Appl. Phys. Lett.* **54**, 60 (1989).
- [32] A. M. Fox, D. A. B. Miller, G. Livescu, and J. E. Cunningham, Quantum well carrier sweep out: Relation to electroabsorption and exciton saturation, *IEEE J. Quantum Electron.* **27**, 2281 (1991).
- [33] X. Marie, T. Amand, J. Barrau, P. Renucci, P. Lejeune, and V. K. Kalevich, Electron-spin quantum-beat dephasing in quantum wells as a probe of the hole band structure, *Phys. Rev. B* **61**, 11065 (2000).
- [34] G. Bastard, *Wave Mechanics Applied to Semiconductor Heterostructures* (John Wiley and Sons Inc., New York, 1990).
- [35] T. Uenoyama and L. J. Sham, Hole Relaxation and Luminescence Polarization in Doped and Undoped Quantum Wells, *Phys. Rev. Lett.* **64**, 3070 (1990).
- [36] Z. Ikonjić, P. Harrison, and A. Valavanis, *Quantum Wells, Wires and Dots: Theoretical and Computational Physics of Semiconductor Nanostructures* (John Wiley & Sons, Ltd., New York, 2016), p. 483.
- [37] E. Wada, Y. Shirahata, T. Naito, M. Itoh, M. Yamaguchi, and T. Taniyama, Inversion of Spin Photocurrent Due to Resonant Transmission, *Phys. Rev. Lett.* **105**, 156601 (2010).
- [38] S. Lach, A. Altenhof, K. Tarafder, F. Schmitt, M. E. Ali, M. Vogel, J. Sauther, P. M. Oppeneer, and C. Ziegler, Metal-organic hybrid interface states of a ferromagnet/organic semiconductor hybrid junction as basis for engineering spin injection in organic spintronics, *Adv. Funct. Mater.* **22**, 989 (2012).
- [39] P. Swanson, T. Tang, M. Givens, L. Miller, T. DeTemple, and J. Coleman, Electroabsorption in single quantum well GaAs laser structures, *Appl. Phys. Lett.* **54**, 1716 (1989).
- [40] M. Dyakonov and V. Y. Kachorovskii, Spin relaxation of two-dimensional electrons in noncentrosymmetric semiconductors, *Sov. Phys. Semicond.* **20**, 110 (1986).
- [41] D. Stich, J. H. Jiang, T. Korn, R. Schulz, D. Schuh, W. Wegscheider, M. W. Wu, and C. Schüller, Detection of large magnetoanisotropy of electron spin dephasing in a high-mobility two-dimensional electron system in a [001]GaAs/Al_xGa_{1-x}As quantum well, *Phys. Rev. B* **76**, 073309 (2007).
- [42] A. Balocchi, Q. H. Duong, P. Renucci, B. L. Liu, C. Fontaine, T. Amand, D. Lagarde, and X. Marie, Full Electrical Control of the Electron Spin Relaxation in GaAs Quantum Wells, *Phys. Rev. Lett.* **107**, 136604 (2011).
- [43] A. Balocchi, T. Amand, G. Wang, B. L. Liu, P. Renucci, Q. H. Duong, and X. Marie, Electric field dependence of the spin relaxation anisotropy in (111) GaAs/AlGaAs quantum wells, *New J. Phys.* **15**, 095016 (2013).
- [44] A. F. Isakovic, D. M. Carr, J. Strand, B. D. Schultz, C. J. Palmstrøm, and P. A. Crowell, Optically pumped transport in ferromagnet-semiconductor Schottky diodes (invited), *J. Appl. Phys.* **91**, 7261 (2002).
- [45] S. Azaizia, A. Balocchi, H. Carrère, P. Renucci, T. Amand, A. Arnoult, C. Fontaine, and X. Marie, Control of the electron spin relaxation by the built-in piezoelectric field in InGaAs quantum wells, *Appl. Phys. Lett.* **108**, 082103 (2016).
- [46] V. L. Korenev, Optical orientation in ferromagnet/semiconductor hybrids, *Semicond. Sci. Technol.* **23**, 114012 (2008).
- [47] L. Meier, G. Salis, C. Ellenberger, K. Ensslin, and E. Gini, Stray-field-induced modification of coherent spin dynamics, *Appl. Phys. Lett.* **88**, 172501 (2006).